

COLLIMATOR PERFORMANCE STUDY AT THE EUROPEAN XFEL

S. Liu[†], F. Brinker, W. Decking, L. Froehlich, N. Golubeva, T. Wamsat, J. Wilgen
 DESY, Hamburg, Germany

Abstract

Beam halo collimation is of great importance for the high repetition rate operation at the European XFEL and for the future CW machines. At the European XFEL several different types of collimators are installed at different locations of the beam line, which include the gun collimators, the bunch compressor collimators, and the main and supplementary collimators in the collimation section. Beam halo measurements have been performed using the wire scanners downstream of the main linac, which show that large part of beam halo is collimated by the gun collimator. Remaining losses in the collimation section are mainly due to misalignment. Alignment using orbit bumps in the collimation section is performed and presented in this paper.

INTRODUCTION

The European XFEL (EuXFEL) operates with a 10 Hz RF gun and a superconducting linac with a maximum repetition rate of 4.5 MHz (27000 bunches/s) and a maximum beam power of more than 500 kW [1-4]. The layout of the EuXFEL is shown in Fig.1 (top). In the future, the EuXFEL is planned to be upgraded to CW operation mode. The long-term stable operation of the facility relies on the control of beam losses and exposure to dark current, which may cause radiation damage of different components in the beam line (e.g. undulators). Therefore, it is crucial to collimate the dark current and beam halos generated in the gun and along the ~ 1.7 km long linac.

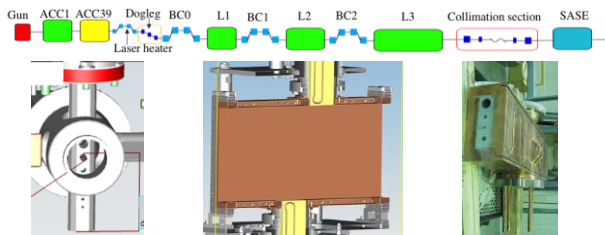


Figure 1: Schematic layout of European XFEL beam line (top) with the gun collimator (bottom left), the bunch compressor collimator (bottom middle) and the main collimator in the collimation section (bottom right).

At the European XFEL several different types of collimators are installed at different locations of the beam line. For the gun dark current and beam halo collimation, two plates (11 mm thick) are installed after the gun (see Fig.1 bottom left): one with \varnothing 2-8 mm variable apertures and another one with fixed \varnothing 8 mm aperture. These two plates

can block main part of the dark current at low energy of 6 MeV and avoid high energy radiation and activation of components. After the injector, in the three bunch compressor (BC) chicanes, three collimators are installed for energy halo collimation. These collimators constitute two bars (upper and lower), which can be moved separately (see Fig.1 bottom middle). The positions of these collimators depend on the compression setup (R56) [5].

After the linac, a ~ 200 m long collimation section (CL section) [6], with four main (COLM) and three supplementary (COLS) collimators, is dedicated to collimate the dark current from the linac, beam halo and off-energy particles. The specifications of the above mentioned collimators are summarized in Table 1.

Table 1: Collimator Specifications

Location	Geometry	Thickness/length	Material
Gun	\varnothing 2-8 mm holes	11 mm	Cu
BC	Upper and lower bars	35 mm/75 mm	Cu
COLM	\varnothing 4,6,8,20 mm holes	0.5 m	Ti alloy
COLS	\varnothing 10 mm holes	1 m	Al

First beam halo¹ measurements using the wire scanners (WS) [7] have been performed before and after the CL section and reported in Ref. [8]. The same method for beam halo measurements is used in this paper to study the performance of the gun collimator. Then, the beam loss map in the CL section is presented followed by the alignment of the beam with respect to the collimators using the orbit bump tool.

GUN COLLIMATOR PERFORMANCE

During the commission of the EuXFEL, we have noticed that a single plate of collimator is not sufficient for the gun dark current collimation, and the secondary particles generated during the collimation can still be transported downstream. Therefore, in the end of 2017, another plate with variable apertures is installed upstream of the fixed aperture plate and it is in operation in the beginning of 2018. After adding this plate, we have observed significant improvement of dark current and beam halo collimation.

¹ By beam halo, we mean the projected beam distribution beyond $\pm 3\sigma$. Since it is the projected beam distribution, it can be the bunch tails which is tilted.

[†] shan.liu@desy.de

Content from this work may be used under the terms of the CC BY 3.0 licence (© 2019). Any distribution of this work must maintain attribution to the author(s), title of the work, publisher, and DOI

Figure 2 shows the beam halo measurements using the WS installed after the main linac, before the CL section. First, the beam core is scanned using the 20 μm thick wire and the signal is collected by the WS detector (scintillating fibers). Then, the beam halo scan is performed using the 50 μm thick wire, and the beam loss monitor (BLM) [9] is used for the signal detection. The beam halo position is then normalized to the beam size unit (number of sigma) extracted from the Gaussian fit of the beam core. The measurements were performed for different gun collimator apertures. One can see that the beam halo level is reduced with smaller collimator apertures, especially in horizontal plane: the halo extension is reduced by $\sim 10\sigma$ by changing the aperture from 6 mm to 5 mm. However, changing from 5 mm to 4 mm didn't make much difference. This may indicate that the residual beam halo is generated downstream of the gun collimator.

Although we can collimate more halo using smaller apertures, it can also generate significant beam loss and transverse wakefield (due to transverse offset). Therefore in normal operation we still use 6 mm aperture.

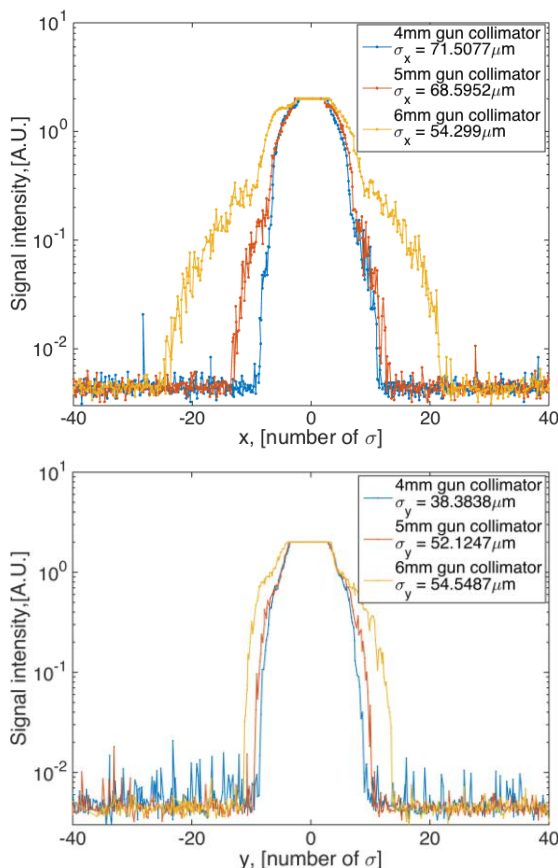


Figure 2: Horizontal (top) and vertical (bottom) beam halo distribution measured after linac and before CL section for different gun collimator apertures.

COLLIMATION SECTION

At the CL section, different optics can be set according to different requirements for beam transportation and beam halo collimation [6]. Optics mode A with a beta

function of ~ 200 m at the collimator location is applied since 2018. The collimation depth with this optics mode is $\sim 20\sigma$ using the 6 mm aperture, which is normally used during the operation.

Since the gun collimator has already collimated the beam halo by large extent, other possible sources for beam losses in the CL section remain energy slope within a bunch train and the misalignment of the beam w.r.t. the collimators. The energy slope can be and has already been controlled by proper LLRF settings. Further improvements on multi-RF flattops setting are on going. Concerning the misalignment, it can generate large transverse kick due to short-range transverse wakefields, which can induce energy spread and projected emittance growth [10]. Therefore, it is important to align the beam through the center of the collimator.

Alignment

For safety reasons, the main collimators are equipped with end switches, which limit the collimator hole movable range to ± 500 μm (vertically) from the vacuum chamber center. Therefore, beyond this range one has to use another tool to align the beam. For this purpose, we have introduced an orbit bump tool. This tool uses the upstream correctors to steer the beam at the collimator location and then uses the downstream correctors to close the orbit variation (see Fig. 3 (left)). The orbit oscillation at the second arc (3rd and 4th collimator position) is due to the transverse kick (transverse momentum) generated by the correctors at the first arc (1st and 2nd collimator position) after 270° phase change. Besides, the horizontal orbit also oscillates at the second arc, this is due to x-y coupling generated by the sextupoles in the first arc³.

During this orbit bump scan, the downstream BLM signals² are recorded, the maximum of which is taken and plotted in Fig. 3 (middle). The recorded signal can be fitted using the error function from the two sides of the distribution:

$$f(x) = 1 \pm \text{erf}(s * (x - p)), \quad (1)$$

where p is the middle position of the error function. The fit is performed separately on the two sides of the distribution and one can define the center of the beam as $(p_{\text{left}} + p_{\text{right}})/2$. In Eq. (1), s is a parameter related to the beam size. Assuming a Gaussian beam in projection, then $s = \sqrt{2}\sigma^2$, however, in the measurements we often observe some beam tails (i.e. slope in the distribution) which prevent us from extracting the beam size from the fit. This tail may indicate that the bunch is tilted at the collimator location. On the other hand, this may be used as a diagnostic for beam tilt generated upstream or inside the CL section.

In Fig. 3 (right) the orbit before and after alignment is shown. Several tests have been done in different weeks

² The BLM signal amplitude is fixed at 2, due to the saturation of the ADC.

³ One can switch them off during the measurement. However, its effect on the measurement is negligible, since the downstream collimators are open (with $\varnothing 20$ mm) during the alignment for the upstream collimators.

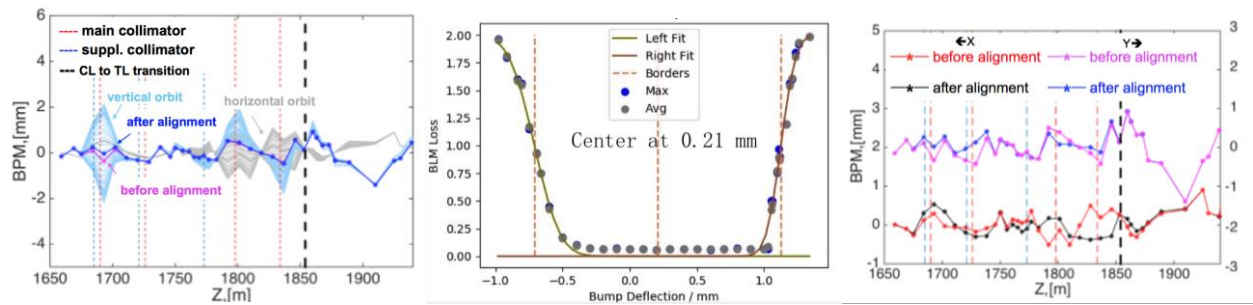


Figure 3: Example of vertical orbit bump scan at the 1st collimator location (left) and the BLM signal as a function of bump deflection strength fitted using Eq. (1) (middle). Horizontal and vertical orbit before and after alignment (right).

and the orbit after alignment is quite reproducible. One can see that at some locations the horizontal offset after alignment is even larger than before alignment (by the readout of the BPM). This may be due to the fact that the collimators can't be moved horizontally.

Beam Halo Measurements After the CL Section

After the alignment in the CL section, one can use the three WSs after the CL section to measure the beam halo (or beam tail). There is 65° phase advance between the 1st and the 2nd one and 25° between the 2nd and the 3rd one. One example of the measurements performed before (top) and after the alignment (bottom) is shown in Fig. 4 for horizontal (left) and vertical (right) plane separately.

In horizontal plane one can see that, after alignment the beam halo measured using different WSs overlap much better than before alignment. This indicates that the beam (including the beam halo or tail part) became almost round in phase space. In the vertical plane, however, the overlap is much worse. The halo part extends much further at one position than the other. Nevertheless, we observe less halo (tail) after alignment than before alignment. This may indicate that, by aligning the beam through the center of the collimator, we have minimized the transverse kick generated by the transverse wakefield.

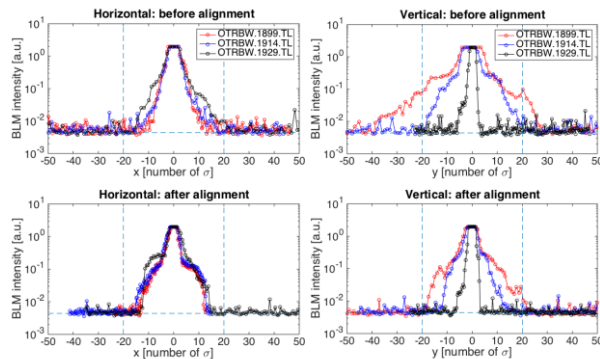


Figure 4: Horizontal (left) and vertical (right) beam halo distribution measured using three different WSs after CL section before (top) and after (bottom) alignment.

CONCLUSIONS AND FUTURE PLANS

Using the gun collimator, we found out that the beam halo extension beyond $\pm 10\sigma$ is generated from the gun,

and can be collimated by the gun collimator (with aperture $< \varnothing 5$ mm).

In the CL section, the remain main losses comes from the misalignment of the beam, especially when the beam is tilted by the transverse wakefield introduced by transverse offset at the collimator location. And during the machine tuning, we have observed that the SASE power depends strongly on careful alignment of the orbit in the CL section. Therefore, alignment is crucial in the CL section. An orbit bump tool is used for this purpose. After automatization, one scan takes around 2 minutes. However, the hysteresis of the correctors and the subsequent orbit variation still need to be taken care of.

After alignment, we used the WSs after the CL section to measure the beam halo (tail). The measurements indicate that the transverse kick generated by the transverse wakefield is minimized by the alignment. Meanwhile, one can use the orbit bump scan and the wire scans as a diagnostic for the beam tail generated by the transverse wakefield.

Up to now, the alignment is only tested for single bunch operation. Optimum position for multi-bunch operation (in case of energy slope within a bunch train) may be different and this can serve as a SASE tuning knob in the future. In addition, further investigations on the transverse kick generated before and after the CL section will be carried out. Theoretical calculations will be compared with the measurements to further develop the orbit bump and wire scans as a new diagnostic for the tilt of the beam tails.

ACKNOWLEDGEMENTS

The authors would like to thank V. Balandin, M. Scholz, D. Noelle, T. Lensch (DESY) for their support in the measurements and fruitful discussions and thanks to F-J. Decker, H-D. Nuhn (SLAC) for sharing their experience and providing valuable comments.

REFERENCES

- [1] M. Altarelli, R. Brinkmann *et al.*, "XFEL: The European X-Ray Free-Electron Laser Technical Design Report", DESY, Hamburg, Germany, DESY 2006-097, 2006.
- [2] H. Weise and W. Decking, "Commissioning and First Lasing of the European XFEL", in *Proc. 38th Int. Free Electron Laser Conf. (FEL'17)*, Santa Fe, NM, USA, Aug. 2017, pp. 9-13. doi:10.18429/JACoW-FEL2017-MOC03

- [3] M. Scholz, “FEL Performance Achieved at European XFEL”, in *Proc. 9th Int. Particle Accelerator Conf. (IPAC'18)*, Vancouver, Canada, Apr.-May 2018, pp 29-33. doi:10.18429/JACoW-IPAC2018-MOZGBD2.
- [4] W. Decking *et al.*, “Status of European XFEL”, presented at the 10th International Particle Accelerator Conf. (IPAC'19), Melbourne, Australia, May. 2019, paper TUPRB020, this conference.
- [5] I. Zagorodnov, M. Dohlus and S. Tomin, “Accelerator beam dynamics at the European x-ray free electron laser”, *Physical Review Accelerators and Beams*, vol. 22, no. 2, Feb. 2019.
doi:10.1103/physrevaccelebeams.22.024401
- [6] V. Balandin, R. Brinkmann, W. Decking, and N. Golubeva, “Optics Solution for the XFEL Post-Linac Collimation Section”, DESY, Hamburg, Germany, TESLA-FEL Report 2007-05, 2007.
- [7] T. Lensch, S. Liu, and M. Scholz, “The European XFEL Wire Scanner System”, in *Proc. 7th International Beam Instrumentation Conference (IBIC'18)*, Shanghai, China, Sep. 2018, pp. 498-500. doi:10.18429/JACoW-IBIC2018-WEPC05
- [8] S. Liu *et al.*, “First Beam Halo Measurements Using Wire Scanners at the European XFEL”, in *Proc. 38th Int. Free Electron Laser Conf. (FEL'17)*, Santa Fe, NM, USA, Aug. 2017, pp. 255-258. doi:10.18429/JACoW-FEL2017-TUP003
- [9] T. Wamsat and T. Lensch, “The European XFEL Beam Loss Monitor System”, in *Proc. 7th International Beam Instrumentation Conference (IBIC'18)*, Shanghai, China, Sep. 2018, pp. 357-360. doi:10.18429/JACoW-IBIC2018-WE0B03
- [10] M. Dohlus, I. Zagorodnov and O. Zagorodnova, “Impedances of collimators in European XFEL”, FEL Report 2010-04.